Routes to spatiotemporal chaos in the rheology of nematogenic fluids

Moumita Das[1],[*] Buddhapriya Chakrabarti[2],[†] Chandan Dasgupta[1], Sriram Ramaswamy[1], and A.K. Sood[1][‡]

[1] *Department of Physics, Indian Institute of Science, Bangalore 560012 INDIA*
[2] *Department of Physics, University of Massachusetts, Amherst, MA 01003*
(Dated: February 2, 2008)

With a view to understanding the "rheochaos" observed in recent experiments in a variety of orientable fluids, we study numerically the equations of motion of the spatiotemporal evolution of the traceless symmetric order parameter of a sheared nematogenic fluid. In particular we establish, by decisive numerical tests, that the irregular oscillatory behavior seen in a region of parameter space where the nematic is not stably flow-aligning is in fact spatiotemporal chaos. We outline the dynamical phase diagram of the model and study the route to the chaotic state. We find that spatiotemporal chaos in this system sets in via a regime of *spatiotemporal intermittency*, with a power-law distribution of the widths of laminar regions, as in H. Chaté and P. Manneville, Phys. Rev. Lett. **58**, 112 (1987). Further, the evolution of the histogram of band sizes shows a growing length-scale as one moves from the chaotic towards the flow aligned phase. Finally we suggest possible experiments which can observe the intriguing behaviors discussed here.

PACS numbers: 61.30.-v,95.10.Fh,47.50.+d

I. INTRODUCTION

The intriguing rheological behavior of solutions of entangled wormlike micelles has been the subject of a large number of experimental and theoretical studies in recent years [1, 2]. These long, semiflexible cylindrical objects, whose length distribution is not fixed by chemical synthesis and can vary reversibly when subjected to changes in temperature, concentration, salinity and flow, have radii $\sim$ 20-25 Å, persistence lengths $\sim$ 150 Å and average lengths upto several microns. Like polymers they entangle above a critical concentration and show pronounced viscoelastic effects. However, unlike covalently bonded polymers, these "living polymers" can break and recombine reversibly in solutions, with profound consequences for stress relaxation and rheology in the form of shear banding[3, 4, 5], and rheological chaos[6, 7, 8, 9, 10, 11, 12]. Measurements [13, 14] report monoexponential relaxation of the viscoelastic response in accordance with the Maxwell model of viscoelasticity. However, for wormlike micelles of CTAT[7, 15] at concentration 1.35 wt.%, the fit to the Maxwell model is very poor, and the Cole-Cole plot deviates from the semi-circular behavior expected in Maxwellian systems and shows an upturn at high frequencies. This deviation from Maxwellian behavior is possibly due to the comparable values of timescales associated with reptation (τ_{rep}) and reversible scission (τ_b) in this system unlike in other wormlike micellar systems where the differences in the time scales $\tau_b << \tau_{rep}$ lead to a 'motional averaging' effect. Further, in the concentrated regime, when the mesh size of the entangled micellar network is shorter than the persistence length of the micelles, orientational correlations begin to appear [5]. In fact the nature of viscoelastic response and the development of long-range orientational order at high concentration play an important role in the non-linear rheology of wormlike micelles, in particular in shear banding transition and rheochaotic behavior[10, 11].

In this paper we explore the dynamical phase diagram of the model studied in [10, 11], with emphasis on the route to spatiotemporal chaos. Our primary finding is summarized in Fig. 1, which shows that this route is characterized by spatiotemporal intermittency. Before presenting our results in more detail, we cover some necessary background material.

The application of large stresses and strains on wormlike micellar solutions can result in a variety of complex rheological behavior. Many dilute solutions of wormlike micelles exhibit a dramatic shear thickening behavior when sheared above a certain threshold rate, often followed by the onset of a flow instability[16, 17, 18]. Experiments have observed shear-banded flow in wormlike micellar solutions with formation of bands or slip layers of different microstructures having very different rheological properties[1, 4, 19, 20, 21, 22, 23]. The shear banding transition is a transition between a homogeneous and an inhomogeneous state of flow, the latter being characterized by a separation of the fluid into macroscopic domains or bands of high and low shear rates. It is associated with a stress plateau (above a certain critical shear rate $\dot{\gamma}_c$ where the shear stress σ versus shear rate $\dot{\gamma}$ curve is a plateau) in the nonlinear mechanical response.

More recently, rheological chaos or "rheochaos" has been observed in experiments studying the nonlinear rheology of dilute entangled solutions of wormlike micelles formed by a surfactant CTAT[6, 7, 15, 24]. Under controlled shear rate conditions in the plateau regime, the shear stress and the first normal stress difference show oscillatory and more complicated, irregular time-
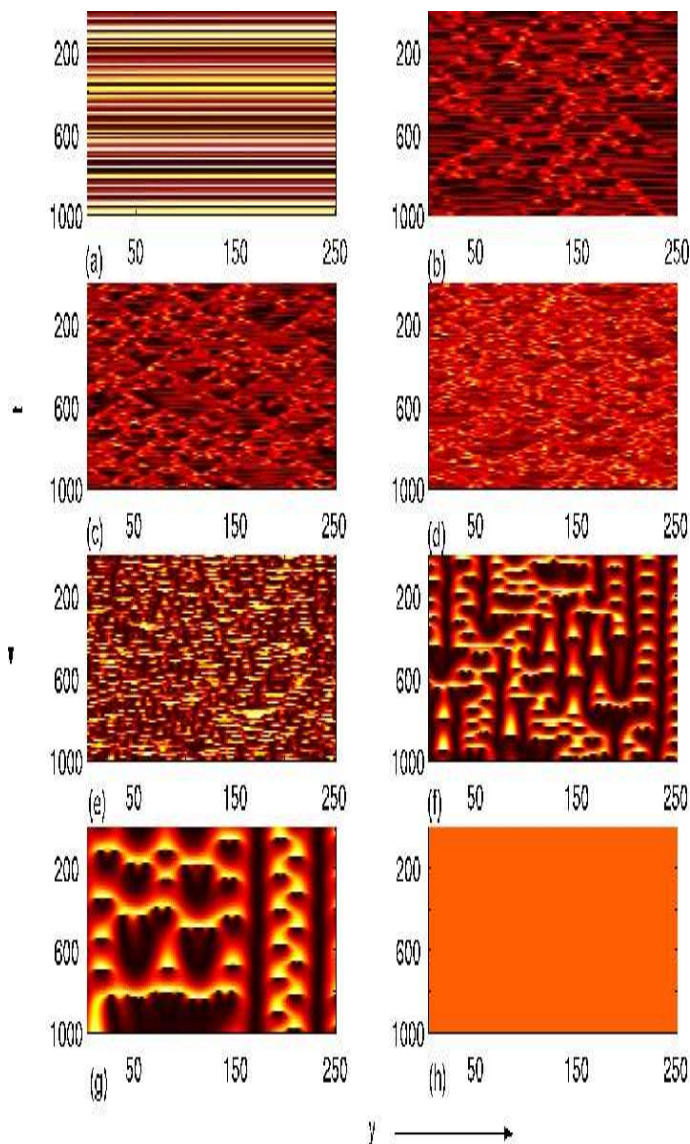
FIG. 1: (Color online) Space-time plots (spatial variation along abscissa and time along ordinate) of the shear stress for $\dot{\gamma} = 4.0$ and (a) $\lambda_k = 1.11$ (time-periodic, spatially homogeneous), (b) to (d), $\lambda_k = 1.12, 1.13, 1.15$ (spatiotemporally intermittent), (e) $\lambda_k = 1.22$ (spatiotemporally chaotic), (f) and (g), $\lambda_k = 1.25$ and 1.27 (chaotic to aligning) and (h) $\lambda_k = 1.28$ (aligned) (colormap used: black(low shear stress) $\rightarrow$ red $\rightarrow$ yellow(high shear stress). Slices taken from system of size $L = 5000$.

dependence. Analysis of the measured time series shows the existence of a positive Lyapunov exponent and a finite non-integer correlation dimension characteristic of deterministic chaos.

Occurrence of sustained oscillations often of an irregular nature have also been reported in some other experiments on complex fluids in shear flow. Roux *et al.*[25, 26] have observed sustained oscillations of the viscosity near the non-equilibrium, layering transition to the "onion" state in a lyotropic lamellar system consisting of close

compact assembly of soft elastic spheres[25, 26, 27]. It has been conjectured that the presence of oscillations in the viscosity is due to structural changes in the fluid, arising out of a competition between an ordering mechanism that is driven by stress and a slow textural evolution which destroys the stress induced ordered state. "Elastic Turbulence" in highly elastic polymer solutions[28] and "Director Turbulence" in nematic liquid crystals in shear flow[29, 30] are two other examples of highly irregular low-Reynolds-number flows in complex fluids. Both these phenomena are characterized by temporal fluctuations and spatial disorder. Also worth noting is the observation by Ramamohan *et al.*[31] of rheochaos in numerical studies of sheared hard-sphere Stokesian suspensions.

Many complex fluids have nonlinear rheological constitutive equations that cannot sustain a homogeneous steady flow. This material instability occurs when the stress vs. strain rate curve is non-monotonic in nature, admitting multiple strain rates $\dot{\gamma}$ at a common stress σ. Particularly for shear flow, it has been shown [32] that homogeneous flow is linearly unstable in a region where the incremental shear viscosity is negative, i.e., $d\sigma/d\dot{\gamma} < 0$. The system then undergoes a separation into two coexisting macroscopic shear bands at different shear rates arranged so as to match the total imposed shear gradient. Systems where the dynamic variables σ or $\dot{\gamma}$ are coupled to microstructural quantities may admit many other possibilities – the flow may never be rendered steady in time, or it may become spatially inhomogeneous even erratic or both. Fielding and Olmsted study one such scenario[9] in the context of shear thinning wormlike micelles where the flow is coupled to the mean micellar length.

Significantly, Grosso *et al.* [33] and Rienäcker *et al.* [34, 35], find temporal rheochaos in the dynamics of the passively advected alignment tensor alone. They study the well-established equations of hydrodynamics for a nematic order parameter, with material constants corresponding to a situation where stable flow alignment is impossible. They consider only spatially *homogeneous* states [36], i.e., they study a set of ordinary differential equations for the independent components of the nematic order parameter, evolving in the presence of an imposed plane shear flow. They are thus not in a position to explore the implications of the observed chaos for shear-banding.

Other theoretical approaches aimed at explaining the rheological chaotic oscillations in a wormlike micellar fluid include those by Cates *et al.*[8]. In the shear thickening regime Cates *et al.*[8] propose a simple phenomenological model for a fluid with memory and an underlying tendency to form shear-banded flows, with only one degree of freedom – the shear stress. Recently Aradian and Cates[37, 38] have studied a spatially inhomogeneous extension of this model, with spatial variation in the vorticity direction. Working at a constant average stress $\langle \sigma \rangle$, they observe a rich spatiotemporal dynamics, mainly seen in what they call "flip flop shear bands" – a low and a high unstable shear band sepa-

rated by an interface and periodically flipping into one another. For a certain choice of parameters they observe irregular time-varying behavior, including spatiotemporal rheochaos. As in our work, the key nonlinearities in [37, 38] arise from nonlinearities in the constitutive relation, not from the inertial nonlinearities familiar from Navier-Stokes turbulence. An important result [37, 38] is that they are able to find complex flow behavior even when the stress vs. shear-rate curve is monotonic. In addition, they find rheochaos even in a few-mode truncation where well-defined shear bands cannot arise.

In this paper we study a minimal model to explain the complex dynamics of orientable fluids, such as wormlike micelles subjected to shear flow. We show that the basic mechanism underlying such complex dynamical behavior can be understood by analyzing the relaxation equations of the alignment tensor of a nematogenic fluid, the underlying idea being that wormlike micelles being elongated objects will have, especially when overlap is significant, a strong tendency to align in the presence of shear. We study equations of motion of the nematic order parameter in the passive advection approximation i.e., ignoring the effect of order parameter stresses on the flow profile which we take to be plane Couette, incorporating spatial variation of the order parameter. We calculate experimentally relevant quantities, e.g, the shear stress and the first normal stress difference, and show that, in a region of shear rates, the evolution of the stresses is spatiotemporally chaotic. Further, in this region the fluid is not homogeneously sheared but shows "dynamic shear banding" (banded flow with temporal evolution of shear bands). A careful analysis of the space-time plots of the shear stress show the presence of a large number of length scales in the chaotic region of the phase space of which only a few dominant ones are selected as one approaches the boundary of the aligned phase. Finally we explore the routes to the spatiotemporally chaotic state. The transition from a regular state (either temporally periodic and spatially homogeneous, or spatiotemporally periodic) to a spatiotemporally chaotic one occurs via a series of spatiotemporally intermittent states. By calculating the dynamic structure factor of the shear stress, and the distribution of the sizes of laminar domains, we can distinguish this intermittent regime from the spatiotemporally chaotic and the regular states occurring in this model. Finally, we present a nonequilibrium phase diagram showing regions where spatiotemporally regular, intermittent and chaotic phases are found.

The paper is organized as follows. In the next section we introduce the model and describe in detail the spatiotemporal chaos that we observe, along with the routes to chaos. We then conclude with a summary and discussions of our results. Our main results on the spatiotemporal nature of rheochaos have appeared in an earlier, shorter article[10].

II. SPATIOTEMPORAL RHEOLOGICAL OSCILLATIONS AND CHAOTIC DYNAMICS IN A NEMATOGENIC FLUID:

A. Model and Methods

Traditionally, complex rheological behaviors such as plateau in the stress vs shear-rate curve[5], shear-banding[3, 4, 5] and "spurt"[39] have been understood through phenomenological models for the dynamics of the stress such as the Johnson-Segalman (JS)[40, 41] model, which produce non-monotonic constitutive relations. In such equations the stress evolves by relaxation or by coupling to the velocity gradient. For example in the JS model the non-Newtonian part of the shear stress $\boldsymbol{\sigma}$ evolves according to

$$\frac{\partial \boldsymbol{\sigma}}{\partial t} + \boldsymbol{u} \cdot \boldsymbol{\nabla} \boldsymbol{\sigma} + \boldsymbol{\sigma}[\boldsymbol{\Omega} - a\boldsymbol{\kappa}] + [\boldsymbol{\Omega} - a\boldsymbol{\kappa}]^T \boldsymbol{\sigma} = 2\mu\boldsymbol{\kappa} - \tau_0^{-1}\boldsymbol{\sigma} \quad (1)$$

with a stress relaxation time τ_0, an elastic modulus μ and a parameter 'a' (called the slip parameter) controlling the non-affine deformation. $\boldsymbol{u}$ is the hydrodynamic velocity field and $\boldsymbol{\Omega}$ and $\boldsymbol{\kappa}$ are the antisymmetric and symmetric parts of the rate-of-deformation tensor. A useful point of view, and one that unifies such phenomenological descriptions with dynamical models of ordering phenomena in condensed matter physics, is that such equations of motion for the stress are not fundamental but are derived from the underlying dynamics of an *alignment tensor* or local nematic order parameter $\boldsymbol{Q}$. Equations of motion for the latter are well-established[42, 43, 44, 45, 46, 47, 48, 49, 50] in terms of microscopic mechanics (Poisson brackets) and local thermodynamics, and naturally include both relaxation and flow-coupling terms of essentially the sort seen, e.g., in the JS model. The contribution of the order parameter $\boldsymbol{Q}$ to the stress tensor is also unambiguous within such a framework, once the free-energy functional $F[\boldsymbol{Q}]$ governing $\boldsymbol{Q}$ is specified. This approach is particularly appropriate when the system in question contains orientable entities, such as the elongated micelles of the experiments of[6, 7, 15, 24]. Thus, not worrying about properties specific to a wormlike micelle, e.g., the breakage and recombination of individual micelles, one can attempt to understand the properties of the wormlike-micelle solution by treating it as an orientable fluid and analyzing the equations of motion of the nematic order parameter. While properties specific to living polymers might play an important role in their rheological behavior, the generality of our order parameter description encourages us to think that we have captured an essential ingredient for rheochaos. As we shall see, this approach leads naturally to terms nonlinear in the stress, absent in the usual JS equations of motion, which lead ultimately to the chaos with which this paper is concerned. Refs. [37, 38] found it necessary to modify the Johnson-Segalman equation by including terms nonlinear in the stress in order to produce chaos.

We now discuss the relaxation equation of the alignment tensor characterizing the molecular orientation of a nematic liquid crystal in shear flow. These equations were derived by various groups [42, 43, 44, 45, 47, 48, 49, 50], using different formalisms resulting in broadly similar though not in all cases identical equations of motion. We work with the equations of[47, 51], so as to make contact with the recent studies[52] of purely temporal chaos in the spatially homogeneous dynamics of nematic liquid crystals in flow. These authors have extended their analysis[34, 35] to include biaxially ordered steady and transient states. Their work has revealed a transition from a kayaking-tumbling motion to a chaotic one via a sequence of tumbling and wagging states. Both intermittency and period doubling routes to chaos have been found.

A nematogenic fluid is comprised of orientable objects, such as rods or discs, with the orientation of the ith particle denoted by the unit vector $\hat{\nu}_i$. In the nematic phase there is an average preferred direction of these molecules, which distinguishes it from the isotropic phase where there is no such preferred direction. The order parameter that measures such apolar anisotropy is the traceless symmetric "alignment tensor" or nematic order parameter

$$\mathbf{Q}_{\alpha\beta}(\mathbf{r}) = \frac{1}{N}\sum_{i=1}^{N}\langle(\nu_\alpha{}^i\nu_\beta{}^i - \frac{1}{3}\delta_{\alpha\beta})\rangle\delta(\mathbf{r}-\mathbf{r}^i). \quad (2)$$

built from the second moment of the orientational distribution function. By construction, it is invariant under $\hat{\nu}_i \rightarrow -\hat{\nu}_i$ and vanishes when the $\hat{\nu}_i$ are isotropically distributed.

Since nematic fluids possess long range directional order, presence of spatial inhomogeneities would result in deformations of the director field and hence cost elastic energy. In general when the variable describing an ordered phase is varying in space, the free energy density will have terms quadratic in $\boldsymbol{\nabla}\mathbf{Q}$. Static mechanical equilibrium for $\mathbf{Q}$ corresponds to extremising the Landau-de-Gennes free-energy functional

$$F[\mathbf{Q}] = \int d^3x[\frac{A}{2}\mathbf{Q}:\mathbf{Q} - \sqrt{\frac{2}{3}}B(\mathbf{Q}\cdot\mathbf{Q}):\mathbf{Q} + \frac{C}{4}(\mathbf{Q}:\mathbf{Q})^2$$
$$+ \frac{\Gamma_1}{2}\boldsymbol{\nabla}\mathbf{Q}\vdots\boldsymbol{\nabla}\mathbf{Q} + \frac{\Gamma_2}{2}\boldsymbol{\nabla}\cdot\mathbf{Q}\cdot\boldsymbol{\nabla}\cdot\mathbf{Q}], \quad (3)$$

with phenomenological parameters A, B and C governing the bulk free-energy difference between isotropic and nematic phases, and Γ_1 and Γ_2 related to the Frank elastic constants of the nematic phase. A macroscopically oriented nematic with axis $\hat{\boldsymbol{n}}$ has $\mathbf{Q} = s(\hat{\boldsymbol{n}}\hat{\boldsymbol{n}} - \mathbf{I}/3)$ (where $\mathbf{I}$ is the unit tensor) which defines the conventional (scalar) nematic order parameter s. For A small enough but positive, F has minima at $s = 0$ and at $s = s_0 \neq 0$. The minimum at $s = s_0$ is lower than the one at $s = 0$ when $A < A_* \equiv 2B^2/9C$ which corresponds to the (mean-field) isotropic-nematic transition. The functional F plays a

key role in the dynamics of $\mathbf{Q}$ as well. The equation of motion for $\mathbf{Q}$ is

$$\frac{\partial\mathbf{Q}}{\partial t} + \mathbf{u}\cdot\boldsymbol{\nabla}\mathbf{Q} = \tau^{-1}\mathbf{G} + (\alpha_0\boldsymbol{\kappa} + \alpha_1\boldsymbol{\kappa}\cdot\mathbf{Q})_{\text{ST}}$$
$$+ \boldsymbol{\Omega}\cdot\mathbf{Q} - \mathbf{Q}\cdot\boldsymbol{\Omega}, \quad (4)$$

where the subscript ST denotes symmetrization and trace-removal. $\mathbf{u}$ is the hydrodynamic velocity field, $\boldsymbol{\kappa} \equiv (1/2)[\boldsymbol{\nabla}\mathbf{u}+(\boldsymbol{\nabla}\mathbf{u})^T]$ and $\boldsymbol{\Omega} \equiv (1/2)[\boldsymbol{\nabla}\mathbf{u}-(\boldsymbol{\nabla}\mathbf{u})^T]$ the shear-rate and vorticity tensors respectively. The flow geometry imposed is plane Couette with velocity $\mathbf{u} = \dot{\gamma}y\hat{x}$ in the $\hat{x}$ direction, gradient in the $\hat{y}$ direction and vorticity in the $\hat{z}$ direction. τ is a bare relaxation time, α_0 and α_1 are parameters related to flow alignment, originating in molecular shapes. $\mathbf{G}$, the molecular field conjugate to $\mathbf{Q}$, is given by

$$\mathbf{G} \equiv -(\delta F/\delta\mathbf{Q})_{\text{ST}} = -[A\mathbf{Q} - \sqrt{6}B(\mathbf{Q}\cdot\mathbf{Q})_{\text{ST}} + C\mathbf{Q}\mathbf{Q}:\mathbf{Q}]$$
$$+ \Gamma_1\nabla^2\mathbf{Q} + \Gamma_2(\boldsymbol{\nabla}\boldsymbol{\nabla}\cdot\mathbf{Q})_{\text{ST}} \quad (5)$$

to the lowest order in a series expansion in powers of $\boldsymbol{\nabla}\mathbf{Q}$.

Since $\mathbf{Q}$ is a traceless and symmetric second rank 3×3 tensor it has five independent components. Accordingly, when the equation of motion of the alignment tensor are appropriately scaled, it is possible to express it in the following orthonormalized basis

$$\mathbf{Q} = \sum_i a_i\mathbf{T}_i,$$
$$\mathbf{T}_0 = \sqrt{3/2}(\hat{\mathbf{z}}\hat{\mathbf{z}})_{\text{ST}},$$
$$\mathbf{T}_1 = \sqrt{1/2}(\hat{\mathbf{x}}\hat{\mathbf{x}} - \hat{\mathbf{y}}\hat{\mathbf{y}}),$$
$$\mathbf{T}_2 = \sqrt{2}(\hat{\mathbf{x}}\hat{\mathbf{y}})_{\text{ST}},$$
$$\mathbf{T}_3 = \sqrt{2}(\hat{\mathbf{x}}\hat{\mathbf{z}})_{\text{ST}},$$
$$\mathbf{T}_4 = \sqrt{2}(\hat{\mathbf{y}}\hat{\mathbf{z}})_{\text{ST}}, \quad (6)$$

and study the equations of motion of each of the components a_k, $k = 0, 1, \ldots, 4$[34, 35] projected out.

It has been observed in the absence of spatial variation that depending on the model parameters entering the equations, the order parameter equations can have different characteristic orbits[34, 35]. Possible in-plane states, where as the name suggests, the director is in the plane of flow determined by the direction of the flow and its gradient, and the order parameter components a_3, $a_4 = 0$ are "Tumbling" (T, in-plane tumbling of the alignment tensor), "Wagging" (W, in-plane wagging) and "Aligning" (A, in-plane flow alignment) states. Out of plane solutions, characterized by non-zero values of a_3 and a_4, observed are "Kayaking-tumbling" (KT, a periodic orbit with the projection of the main director in the shear plane describing a tumbling motion), "Kayaking-wagging" (KW, a periodic orbit with the projection of the main director in the shear plane describing a wagging motion) and finally "Complex" (C) characterized by complicated motion of the alignment tensor. This includes periodic orbits composed of sequences of KT and

KW motion and chaotic orbits characterized by a positive largest Lyapunov exponent.

A solution phase diagram based on the various in-plane and out-of-plane states for $A = 0$ and $\alpha_1 = 0$ is given in[35]. It is observed that $\alpha_1 \neq 0$ gives similar results[12]. As control parameters, we use $\lambda_k \equiv -(2/\sqrt{3})\alpha_0$ related to the tumbling coefficient in Leslie-Ericksen theory[34, 35], and the shear rate $\dot{\gamma}$ to study the phase behavior of this system.

It is observed in experiments that the flow curve (shear stress *vs* strain rate) of a wormlike micellar system in shear flow has a rather large plateau region where banded flow is believed to occur, and a study of the dynamics of traceless symmetric order parameter **Q** (Eq.4) for a sheared nematogenic system, that allows spatial variation, is likely to capture this feature. As we shall see later the shear banding observed in such systems is dynamic in nature and is an important element in the spatiotemporal rheochaos we observe.

Hereafter we express the equations in the orthonormalised basis as in Eq.6. As in[34, 35], we rescale time by the linearized relaxation time τ/A_* at the mean-field isotropic-nematic transition, and **Q** as well by its magnitude at that transition. We have set $\alpha_1 = 0$ in our analysis as it seems to have little effect on the dynamical behavior of the system[12, 34, 35] in the parameter range studied. Further, we choose $A = 0$ throughout, to make a correspondence to the ODE studies of [34, 35]. This places the system well in the nematic phase at zero shear, in fact at the limit of metastability of the isotropic phase. Distances are non-dimensionalized by the diffusion length constructed out of Γ_1 and τ/A_*. The ratio Γ_2/Γ_1 is therefore a free parameter which we have set to unity in our study.

The resulting equations are then numerically integrated using a fourth order Runge-Kutta scheme with a fixed time step ($\Delta t = 0.001$). For all the results quoted here a symmetrized form of the finite difference scheme involving nearest neighbors is used to calculate the gradient terms. Thus

$$\nabla^2 f_i = \frac{f_{i+1} + f_{i-1} - 2f_i}{(\Delta x)^2}$$
$$\nabla f_i = \frac{f_{i+1} - f_{i-1}}{2\Delta x} \qquad (7)$$

We have checked that our results are not changed if smaller values of Δt are used. We have further checked that the results do not change if the grid spacing is changed (i.e. Δx is decreased) and more neighbors to the left and right of a particular site in question are used to calculate the derivative. This gives us confidence that the results quoted here do reflect the behavior of a continuum theory and are not artifacts of the numerical procedure used. We use boundary conditions with the director being normal to the walls. With this, we discard the first 6×10^6 timesteps to avoid any possibly transient behavior. We monitor the time evolution of the system for the next 5×10^6 time steps (i.e. $t = 5000$), recording con-

figurations after every 10^3 steps. We have carried out the study with system sizes ranging from $L = 100$ to $L = 5000$.

Further, we calculate the contribution of the alignment tensor to the deviatoric stress[35, 53, 54, 55] $\boldsymbol{\sigma}^{OP} \propto \alpha_0 \mathbf{G} - \alpha_1 (\mathbf{Q} \cdot \mathbf{G})_{ST}$ where **G**, defined in (Eq.5), is the nematic molecular field, and the total deviatoric stress is $\boldsymbol{\sigma}^{OP}$ plus the bare viscous stress. Since the latter is a constant within the passive advection approximation, we can study the rheology by looking at $\boldsymbol{\sigma}^{OP}$ alone. We are aware of the importance of allowing the velocity profile to alter in response to the stresses produced by the order parameter field, and this is currently under study [56].

While generating the results for the time-series analysis for the LS, we run the simulation till $t = 20000$, for $L = 5000$ sized system, recording data at space points at intervals of $l = 10$. We monitor the space-time evolution of the shear stress (the xy component of the deviatoric stress $\boldsymbol{\sigma}^{OP}$) (referred to as Σ_{xy}) and the first and second normal stress differences $\Sigma_{xx} - \Sigma_{yy}$ and $\Sigma_{yy} - \Sigma_{zz}$ respectively.

B. Results and Discussion

1. Phase Behavior and Dynamic Shear Banding

In view of prior work on observation of chaos in the local equations of motion of the alignment tensor (spatially homogeneous version of Eq.4) by Rienäcker *et al.*[34, 35] we address the following question: Is the phase diagram (in the $\dot{\gamma} - \lambda_k$ plane) affected by allowing spatial variation of the order parameter ? We answer this question in affirmative, and show that the 'C' region of the phase diagram of Rienäcker *et al.*[34, 35] corresponding to "complex" or chaotic orbits *broadens* upon incorporating the spatial degrees of freedom. In other words, there exist parameter ranges where the spatially homogeneous system is not chaotic, but chaos sets in once inhomogeneity is allowed. A result of particular interest is the observation of "spatiotemporally intermittent" (STI) states in a certain range of parameters *en route* from the regular to the spatiotemporally chaotic regimes. Such behavior is by definition not accessible in the evolution equations of the spatially homogeneous alignment tensor studied in [34, 35]. It would be of interest to find chaotic regimes where only two of the five independent components of **Q** are nonzero. Since the number of degrees of freedom per space-point would then be two, such chaos would clearly be a consequence of spatial coupling. We have not located such a regime so far.

Local phase portraits (orbits obtained when various pairs of order parameter components are plotted against each other) illustrate the chaotic or orderly nature of the on-site dynamics. Shown in the right panels of Fig.2 are the local phase portraits (a_1 vs a_0) for a particular point x_0 for various values of the tumbling parameter λ_k, obtained by holding the shear-rate fixed at $\dot{\gamma} = 3.5$. We
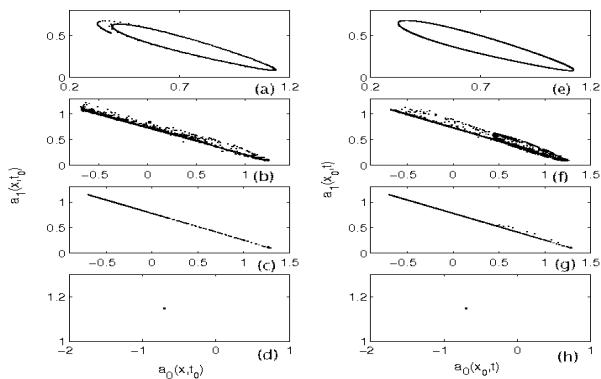
FIG. 2: Plots showing $a_0(x,t_0)$ vs $a_1(x,t_0)$ (left panel) and $a_0(x_0,t)$ vs $a_1(x_0,t)$ (right panel) for Periodic [(a),(e)], Chaotic [(b),(f)], (C→A) [(c),(g)] and aligned [(d),(h)] regimes.

FIG. 3: (Color online) Space-time behavior of the shear stress in the chaotic regime, $\dot\gamma$=3.678 and λ_k=1.25. Slice taken from a system of size $L = 5000$.

FIG. 4: (Color online) Space-time behavior (surface plots) of the shear stress in the chaotic to aligning regime, $\dot\gamma = 4.05$ and λ_k=1.25. Slice taken from a system of size $L = 5000$.

have checked that the character of the phase portrait remains intact upon going from one space point to another though in the chaotic regime there is no phase coherence between two such portraits. A closed curve corresponding to a limit cycle is seen at $\lambda_k = 1.27$, while at $\lambda_k = 1.3$ (corresponding to the 'C' region of the phase space) it is space filling. At $\lambda_k = 1.35$, as one approaches the region where the director aligns with the flow the points reduce to those on a line and eventually in the aligning regime ($\lambda_k = 1.365$) where the director has already aligned with the flow it is represented by a point. This assures us that the local dynamics in the spatially extended case is similar to that of the ODEs of[34, 35].

We also construct the spatial analogues of these portraits, i.e., we allow the system to evolve till a sufficiently long time (say t_0) and then record the spatial series. Again we get a limit cycle in the 'T' region of [34, 35],, followed by a space-filling curve in the 'C' region. As we go from the Chaotic towards the Aligning regime, the points arrange themselves on a line, and finally in the aligned regime one only obtains a point, corresponding to a spatially uniform state. This is shown in the left panel for Fig.2. One should note here that the 'T' regime here corresponds to spatiotemporally periodic states whereas in other regions of parameter space one does observe states that are temporally periodic but spatially homogeneous (Fig. 1 (a)) and for such states the local phase portrait corresponding to spatial variation at a fixed time would be a point and not be a closed curve.

We now turn to the detailed spatiotemporal structure of the phase diagram of this system. We find many interesting phases including spatiotemporally chaotic states with a broad distribution of length scales (Figs.1(e),3), spatiotemporally irregular states in which a few length scales are picked up by the system (Figs.1(f) and (g), 4), a flow aligned phase (Fig. 1(h)) and also regular states (R) showing periodicity in both in time and space (Fig.5) or that are periodic in time and homogeneous in space (Fig.1(a)). In addition to these states we find the
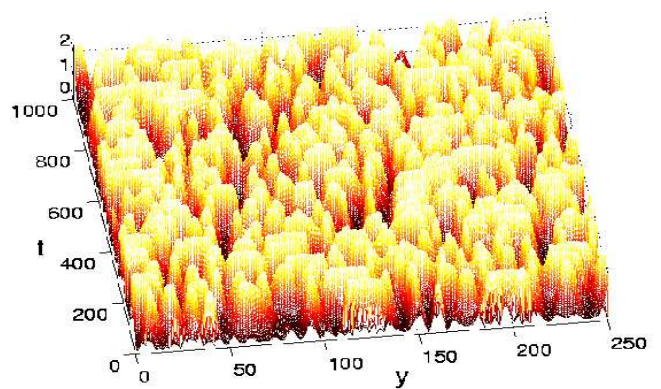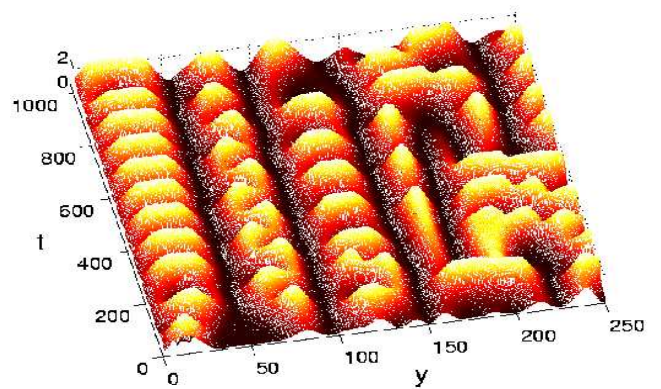
presence of spatiotemporally intermittent states (STI) (Fig.1(b) and (c)). In regions of parameter space we have also observed spatially and temporally ordered domains co-existing with patches characteristic of STI.(Fig.6). The parameter values at which these are seen, correspond well with those obtained from the phase diagram of[34, 35].

Let us now focus on the parameter region labelled 'C' or 'Complex' in[34, 35], where we find spatiotemporal chaos. This regime is characterized by dynamic instability of shear bands as seen in Fig.3 which shows several distinct events, such as the persistence, movement, and abrupt disappearance of shear bands. It is found that the typical length scale at which banding occurs is a fraction of the system size, though it follows a broad distribution. As one moves closer to the phase boundary separating the spatiotemporally chaotic state from stable flow alignment, the bands become more persistent in time and larger in spatial extent as shown in Fig.4.

We have computed the distribution of band sizes or spatial "stress drops", and looked for the presence of dominant length-scales in the system in order to obtain
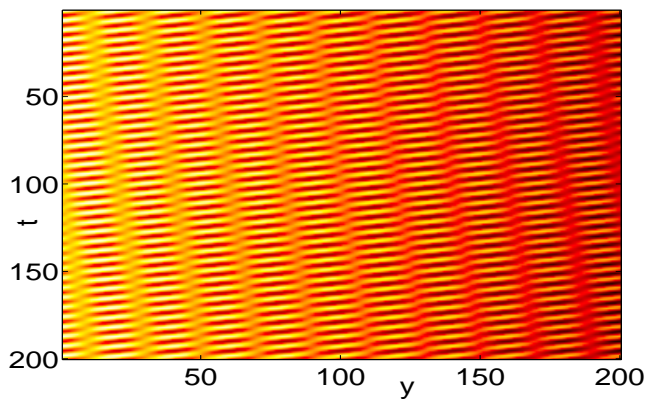
FIG. 5: (Color online) The space-time correlation function in a regime which is both spatially and temporally periodic. $\dot{\gamma}=3.4, \lambda=1.29$
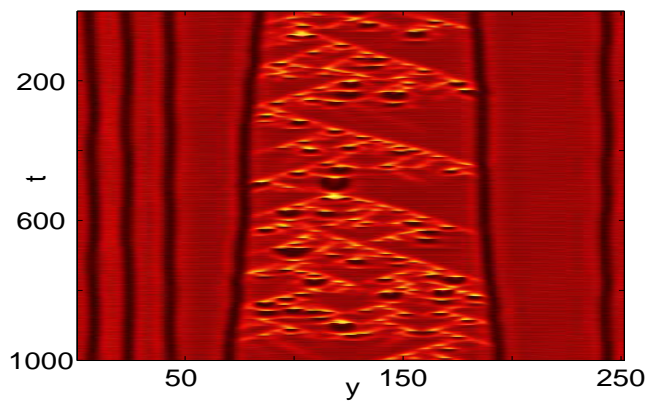

FIG. 6: (Color online) Space-time evolution of the shear stress showing co-existence of different dynamical regimes at $\dot{\gamma}=3.9, \lambda=1.12$.
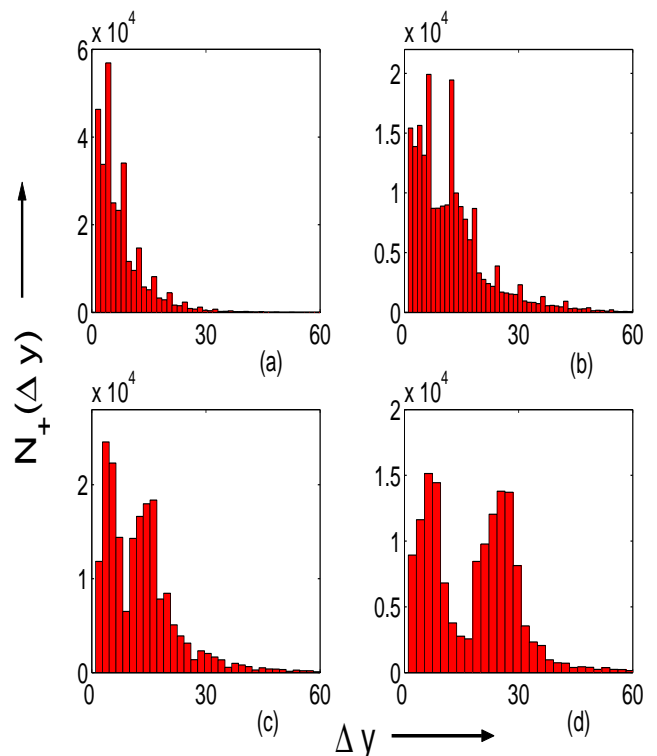

FIG. 7: (Color online) Spatial distribution of "stress drops" (corresponding to residence intervals in which the shear stress is above a threshold $\Sigma_{0xy} = 0.8$) in the Chaotic (a) and $C \rightarrow A$ (b,c,d) regimes. $\dot{\gamma} = 4.0$ and $\lambda_k = 1.22$ (a),1.24 (b),1.25 (c), 1.27 (d).

dominant length-scale associated with the shear bands increases.

2. Route to the Spatiotemporally Chaotic State

We now monitor the approach to the spatiotemporally chaotic state as a function of the tumbling parameter λ_k, for a fixed value of $\dot{\gamma}$ (= 3.8). We observe a sequence of states. At low λ_k (1.0), the shear stress is periodic in time and homogeneous in space Fig.1(a). As we increase λ_k, we come across states which are both spatially and temporally disordered, (Figs.1 (b) and (c)) consisting of propagating disturbances in a background of highly irregular local structures, which resemble geometric patterns seen in probabilistic cellular automata [57]. The borders of the ordered regions evolve like fronts towards each other until this region eventually disappears in the chaotic background. These states are typical of what is known as "spatiotemporal intermittency" (STI)[58, 59, 60, 62]. Indeed, it is suggested [60, 65] that the transition to fully developed spatiotemporal chaos generally occurs via this admixture of complex irregular structures (high shear stress) intermittently present with more regular low shear regions. In contrast to low dimensional systems where intermittency is restricted to tem-

a better understanding of the disorderly structure of the shear bands as seen in Fig.3, and compared it with the behavior seen close to the phase boundary (Fig.4). Another important reason for such an analysis is to rule out any hidden periodicity that might be present in the space-time profiles of shear stress as shown in Fig.3.

The "stress drop" calculation is outlined below. At a given time (say t_i), we define a threshold Σ_{0xy}, a little above the global mean $\langle \Sigma_{xy} \rangle_{y,t}$, and map the spatial configuration to a space-time array of ± 1: $\tilde{\Sigma}_{xy} = \text{sgn}(\Sigma_{xy} - \Sigma_{0xy})$. Fig.7 shows the histogram of the spatial length of intervals corresponding to the +state, for the Chaotic and the Chaotic to Aligning ($C \rightarrow A$) regimes. We have considered configurations extending over $L = 2500$ spatial points, and the statistics is summed over configurations sampled at 5000 times (i.e. $i = 1, 5000$). As expected, the distribution of band lengths in the spatiotemporally chaotic regime is fairly broad and roughly exponential in shape, whereas as one approaches the Aligning regime, the distribution is peaked about a few dominant length-scales. Also, note that as one passes from the Chaotic to the Chaotic-to-Aligning (C → A) state, the

poral behavior, STI manifests itself as a sustained regime where coherent-regular and disordered-chaotic domains coexist and evolve in space and time. Earlier studies of the onset of spatiotemporal chaos [58, 59, 60, 61, 62, 63] suggest a relation to directed percolation (DP). Evidence for DP-like behavior in spatiotemporal intermittency mostly comes from studies of coupled map lattices (CML)[62]. Such processes are modeled as a probabilistic cellular automaton with two states per site, inactive and active, corresponding respectively to the laminar and chaotic domains in the case of STI. Studies find that in the STI regime, a laminar (inactive) site becomes chaotic (active) at a particular time only if at least one of its neighbors was chaotic at an earlier time, there being no spontaneous creation of disordered-chaotic sites. Hence a disordered site can either relax spontaneously to its laminar state or contaminate its neighbors. This feature is analogous to directed percolation, and one consequence of this picture is the presence of an absorbing state: in STI studies of CMLs, once all the sites relax spontaneously to the laminar state, the system gets trapped in this state forever, thus the laminar state in STI corresponds to an absorbing state in DP. This analogy predicts that STI should show critical behavior similar to that associated with DP - power law growth of chaotic domains, and characteristic static and spreading exponents. There is however still no uniformity of opinion on whether spatiotemporal intermittency belongs to the same universality class as DP as characterised by the critical exponents of the DP class. Some studies of coupled map lattices [58], PDEs [65, 67] and experiments [66] suggest that, though the critical behavior in STI is visually similar to DP, the exponents measured in STI are not universal. Other investigations that have evaluated the exponents at the onset of spatiotemporal intermittency in coupled circle map lattices[62] and in experimental systems [64], claim that this transition indeed falls in the universality class of directed percolation. Our aim in this context is to macroscopically characterize the disordered structures in the spatiotemporally intermittent state in terms of the distribution of the widths of the laminar domains and study the qualitative connection between STI and DP. Accordingly, following the analysis in Chaté *et al.* [58, 65] we study the decay of the distribution of laminar domains at the onset of intermittency and far away from this onset. At each time-step, the spatial series of the shear stress values are scanned, and the widths of the laminar regions (regions for which the spatial gradient is less than a sufficiently small value) are measured and inserted into a histogram. This process is then cumulated over time, giving the distribution of laminar domains. Previous studies have found that at the onset of spatiotemporal intermittency, this distribution has a power law decay (with a power ranging from 1.5 to 2.0 in CML studies [58] and experiments [66] and 3.15 in a variant of the Swift-Hohenberg eqn. [65]), while away from the onset, it has an exponential decay. We find a similar behavior. In our work, at a representative point
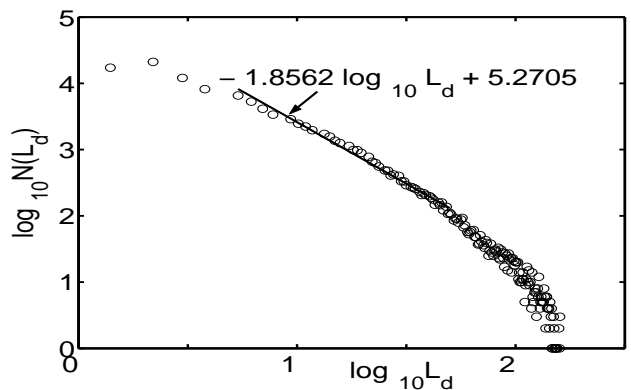

FIG. 8: Decay of the distribution of laminar domains at the onset of the spatiotemporal intermittent regime (represented by circles) on Log-Log scale. The solid line is a power law fit to the data with an exponent $\psi_{STI} = 1.86 \pm 0.05$.
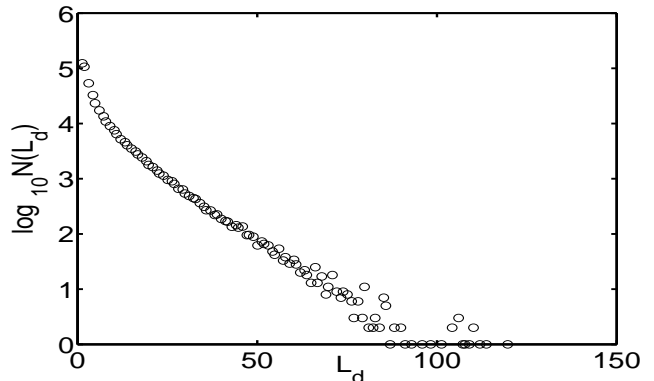

FIG. 9: Decay of the distribution of laminar domains away from the above-mentioned onset and well within the STI regime (represented by circles) on a semiLog scale.

($\dot{\gamma} = 3.9$, $\lambda_k = 1.116$) at the onset of intermittency, the distribution of laminar domains has a power law decay (Fig. 8), with an exponent of 1.86 and a standard deviation from the data of 0.05. Away from this onset ($\dot{\gamma} = 4.0$, $\lambda_k = 1.13$), the decay is close to exponential as evident from Figure 9.

Another way of characterizing the time evolution of the coherent and disorderly regions in the spatiotemporally intermittent states of Figs.1 (b) and (c) is to calculate the dynamical structure factor for the shear stress. Fig.10 shows the dynamic structure factor characteristic of this regime. When the system is in the flow aligned regime $S(k,\omega)$ has a peak at $k = 0$ and $\omega = 0$. On the other hand in the spatiotemporally intermittent state, the dominant weight in $S(k,\omega)$ is on lines of $\omega \propto \pm k$, implying disturbances with a characteristic speed of propagation. The front velocity of the cellular automata like patterns seen in the space-time plots in this regime can be calculated from the slope of these lines. In Figs.1 (d) and (e), the system is in the chaotic regime. As we pass on from the chaotic towards the aligning regime, more regular struc-
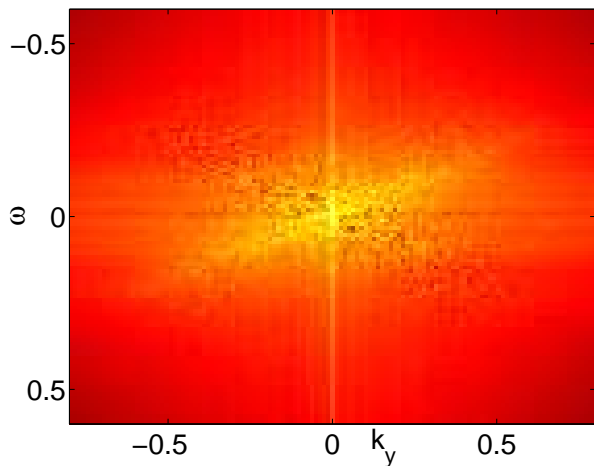
FIG. 10: (Color online) Pseudocolor plot of the dynamic structure factor $S(k_y, \omega)$ in the "STI" (spatiotemporally intermittent) regime. Color at any point $\sim$ logarithm (to base 10) of the value of $S(k_y, \omega)$ at that point.
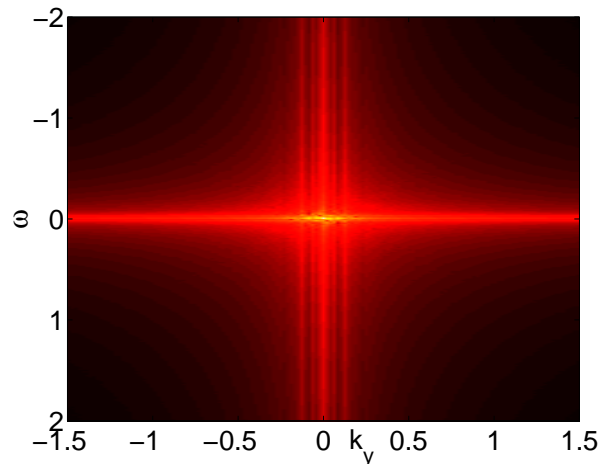

FIG. 12: (Color online) Dynamic structure factor in the $C \rightarrow A$ regime. The system has almost relaxed to a steady state in time, and spatially there are large domains that are flow aligned.
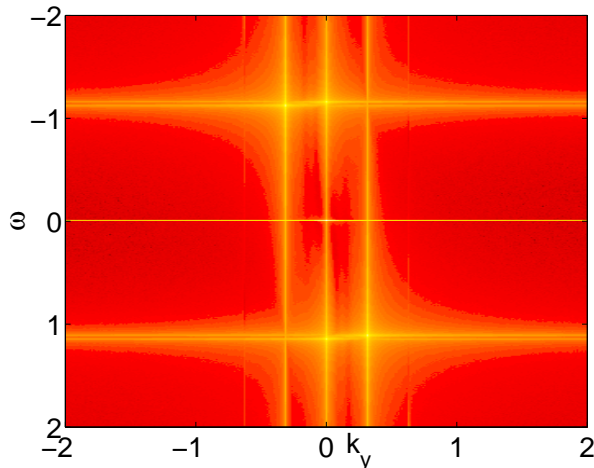

FIG. 11: (Color online) Dynamic structure factor in the spatiotemporally periodic regime. The peridicity in time and space is borne out by the straight lines parallel to the frequency and wave-vector axes respectively.
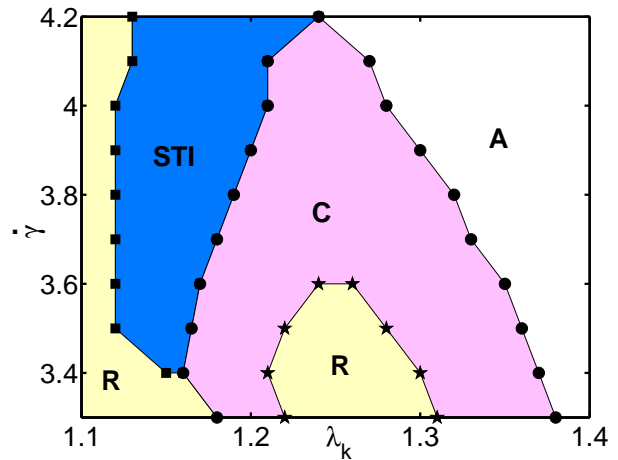

FIG. 13: (Color online) Phase diagram of the system in the λ_k vs $\dot{\gamma}$ plane, showing regular, i.e., periodic in time and either periodic or homogeneous in space (R), chaotic (C), aligning (A) and spatiotemporally intermittent (STI) regimes. Note the reentrant chaotic behavior as a function of $\dot{\gamma}$ in a narrow region of λ_k and as a function of λ_k for $\dot{\gamma} < 3.6$.

tures are seen to evolve (Figs.1 (f), (g)); the shear bands grow in spatial extent and are more long-lived. Fig.1 (h) shows a snapshot of the shear stress in the flow aligned regime. Figures 11 and 12 show the dynamical structure factor in the spatiotemporally periodic regime and close to the chaotic-aligning phase boundary respectively.

Finally, we present the phase diagram coming out of the previous analysis as in the Fig.13. The phase diagram was calculated by monitoring the shear stress profile as well as various components of the nematic order parameter (as they are strikingly different for the different phases, which is also borne out by the difference in the corresponding dynamic structure factors) as a function of the shear rate $\dot{\gamma}$ and the tumbling parameter λ_k.

3. Lyapunov structure of the Chaotic State

Next we try to characterize the chaotic states in our study. In studying dynamics of spatio-temporal systems [68], one needs to establish whether the system is truly in a spatiotemporally chaotic regime or can be described by a model with only a few (dominant) independent modes. So from the multivariate time-series generated by such systems, one tries to compute quantities analogous to the invariant measures used to characterize low dimensional chaos. However, true spatiotemporal chaos corresponds to spatially high dimensional attractors, with dimension growing with the system's spatial extent, and the esti-

mation of invariants such as the correlation dimension can be quite problematic. Indeed we find that the chaos that we observe is quite high dimensional (embedding dimension[69, 70] $m \geq 10$). A reliable estimate of the correlation dimensions can be made only from a data train so long as to require prohibitively large computational times to generate.

An alternative approach is to study the Lyapunov spectrum (LS). For a discrete N dimensional dynamical system, there exist N Lyapunov exponents corresponding to the rates of expansion and/or contraction of nearby orbits in the tangent space in each dimension. The LS is then the collection of all the N Lyapunov exponents $\lambda_i, i = 1 : N$, arranged in decreasing order. The LS is very useful in the characterization of a chaotic attractor. Useful quantities that can be calculated from the LS are the number of positive Lyapunov exponents N_{λ_+} and sum of the positive Lyapunov exponents $\sum_{\lambda_+}$. In fact the sum of the positive Lyapunov exponents provides an upper bound for the so called Kolmogorov-Sinai entropy h which quantifies the mean rate of growth of uncertainty in a system subjected to small perturbations. In many cases, h is well approximated by the sum $\sum_{\lambda_+}$ [71]. Both these quantities have been found to scale extensively with system size in spatiotemporally chaotic systems. For dynamical systems with only a few effective degrees of freedom, it is straightforward to compute the LS. However for extended systems with a large number of degrees of freedom, even a few hundred, it runs into severe difficulties because of the inordinately large computing time and memory space required. In such situations it is important to make use of techniques that derive information about the whole system by analyzing comparatively small systems with exactly the same dynamical behavior [72, 73, 74]. It has been widely observed that the LS for spatiotemporal systems is an extensive measure [75] and is associated with a rescaling property [72, 73, 74] i.e., the LS of a subsystem, when suitably rescaled can give rise to the LS of the whole system [76]. The volume rescaling property for the LS in spatiotemporally chaotic systems also implies that extensive (size dependent) quantities such as $\sum_{\lambda_+}$ and N_{λ_+} scale with not only the system size but also the subsystem size. Hence, instead of trying to study the spectrum and related quantities in a system of large size N, one could confine the analysis to relatively small, more manageable subsystems of size N_s i.e., at space points j in an interval $i_0 < j < i_0 + N_s - 1$ (where i_0 is an arbitrary reference point), and study the scaling of related quantities with subsystem size N_s[69]. Thus, instead of trying to implement the correlation-dimension method for our spatially extended problem, we study the LS [69, 77]. Further, instead of studying systems of ever-increasing size, we look at subsystems of size N_s in a given large system of size N.

For spatiotemporal chaos we expect to find that the number of positive Lyapunov exponents grows systematically with N_s. This is seen in Fig.14. For both figures in Fig.14 , we carry out the procedure with two different
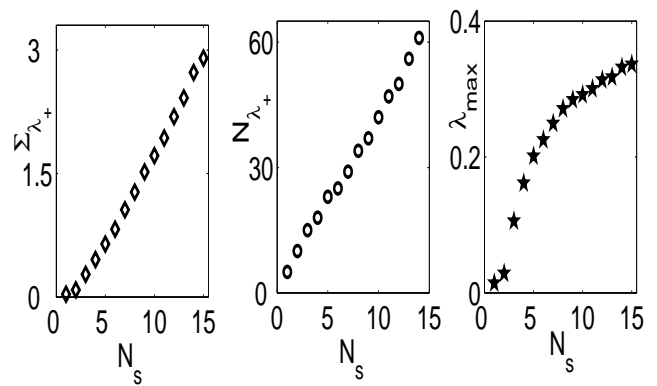

FIG. 14: Sum of positive Lyapunov exponents (left panel), Number of positive Lyapunov exponents (middle panel) and the largest Lyapunov exponent (right panel) as functions of subsystem size N_s, for $\dot{\gamma} = 3.678$, $\lambda_k = 1.25$. Embedding dimension for the time series of each space point is 10.(i_0=101, see text).

reference points i_0 and find essentially the same curves. Furthermore, it has been reported in many studies of spatiotemporally chaotic systems[72, 73, 74] that when calculating the subsystem LS for increasing subsystem size N_s, one finds that the Lyapunov exponents of two consecutive sizes are interleaved, i.e. the ith Lyapunov exponent λ_i for the sub-system of size N_s lies between the ith and $(i+1)$th Lyapunov exponent of the subsystem of size $N_s + 1$. A direct consequence of this property is that with increasing subsystem size N_s, the largest Lyapunov exponent will also increase, asymptotically approaching its value corresponding to the case when the subsystem size is of the order of the system size. This trend is clearly seen in Fig.14 (b).

C.   Conclusions

In summary, we have proposed a mechanism by which one might explain the chaotic and irregular rheological response of soft materials in shear flow, wormlike micelles in particular. The main idea brought out in this paper is that the coupling of orientational degrees of freedom in a complex fluid with hydrodynamic flow can lead to spatiotemporal chaos for low Reynolds number flows. In particular, we have demonstrated that the nonlinear relaxation of the order parameter in nematogenic fluids, together with the coupling of nematic order parameter to flow, are key ingredients for rheological chaos. The broad idea that nonlinearities in the stress and spatial inhomogeneity are essential is a feature that our work shares with [9] and [37, 38].

We should note here that there could be more than one mechanism at work in producing rheochaos. The mechanism observed in our study is that the system exhibits chaos in its local temporal dynamics, and then these localized regions mutually interact with one another to gen-

erate spatial disorder. Fielding *et al.* [9] however have found spatiotemporally chaotic rheological behavior in a model system whose local dynamics does not show chaos, but incorporating the spatial degrees of freedom makes it chaotic. Note also that in the parameter range we have studied so far the equilibrium phase of the system, in the absence of shear, is nematic. We made this choice to facilitate comparison with the work of [34, 35]; a better choice from the point of view of the experiments on wormlike micelles would be to work in the isotropic phase, with a substantial susceptibility to nematic ordering. We do not know if shear produces chaos in that situation, although it seems likely. It is also worth investigating whether nematics with stable flow-alignment at low shear-rates can go chaotic at higher rates of flow. That the structures in the transitional region between order and spatiotemporal chaos are similar to those in directed percolation, as in some other systems undergoing the transition to spatiotemporal chaos, is interesting and suggests a direction for possible experimental tests.

We now comment on experiments which can test some of the ideas proposed in this paper. The dynamics of the alignment tensor can be studied in rheo-optical experiments on dichroism[78], flow birefringence and rheo-small angle light scattering[79]. Flow birefringence experiments carried out in the last decade have shed light on shear banding and orientational properties of micellar solutions [5]. Small angle neutron scattering experiments, using a two-dimensional detector, have also been used to analyse the orientational degrees of a micellar fluid in shear flow: the presence and proportions of the isotropic and nematic phases under shear, as well as the order parameter of the shear induced nematic phase in such systems have been studied [5]. In order to investigate rheochaotic behavior in space and time in systems such as under consideration, one could use these rheo-optical techniques and try to look for the irregularities in the spatial distribution of band sizes and their temporal persistence, in a regime in the nematic phase where the micelles are not flow aligned. Further, very recently, spatio-temporal dynamics of wormlike micelles in shear flow has been studied using high-frequency ultrasonic velocimetry[23], and various dynamical regimes including slow nucleation and growth of a high-shear band and fast oscillations of the band position have been observed, though the complex fast behavior reported is not chaotic.

[1] R. Larson, *The Structure and Rheology of Complex Fluids*, (Oxford University Press, New York, 1999).

[2] J. N. Israelachvili, *Intermolecular and Surface Forces: With Applications to Colloidal and Biological Systems*, (Academic, London, 1985).

[3] R. Makhloufi, J.-P. Decruppe, A. At-Ali, R. Cressely, Europhys. Lett. **32**, 253 (1995).

[4] R. W. Mair, and P. T. Calaghan, Europhys. Lett. **36**, 719 (1996).

[5] J. -F. Berret, cond-mat/0406681.

[6] R. Bandyopadhyay, G. Basappa, and A. K. Sood, Pramana **53**, 223 (1999).

[7] R. Bandyopadhyay, G. Basappa, and A. K. Sood, Phys. Rev. Lett, **84** 2022, (2000).

[8] M. E. Cates, D. A. Head, and A. Ajdari, Phys. Rev. E **66**, 025202 (2002).

[9] S. M. Fielding and P. D. Olmsted, Phys. Rev. Lett. **92**, 084502 (2004).

[10] B. Chakrabarti, M. Das, C. Dasgupta, S. Ramaswamy and A. K. Sood, Phys. Rev. Lett **92**, 055501 (2004).

[11] M. Das, R. Bandyopadhyay, B. Chakrabarti, S. Ramaswamy, C. Dasgupta and A. K. Sood, *Molecular Gels* ed. P. Terech, and R. G. Weiss (Kluwer), (to appear).

[12] B. Chakrabarti, Ph D Thesis, Indian Institute of Science, unpublished (2003).

[13] H. Rehage, H. Hoffmann,J. Phys. Chem. **92**, 4712 (1988); T. Shikata, K. Hirata, T. Kotaka, Langmuir **4**, 354 (1988); T. Shikata, K. Hirata, T. Kotaka, Langmuir **5**, 398 (1989); F. Kern, R. Zana, S.J. Candau, Langmuir **7**, 1344 (1991); A. Khatory, F. Lequeux, F. Kern, S.J. Candau, Langmuir **9**, 1456 (1993).

[14] H. Rehage, and H. Hoffmann, Mol. Phys. **74**, 933 (1991)

[15] R. Bandyopadhyay, Ph D Thesis, Indian Institute of Science, unpublished (2000).

[16] Y. Hu, P. Boltenhagen, E. Matthys, and D. J. Pine, J. Rheol. **42**, 1209 (1998).

[17] I. A. Kadoma, and J. W. van Egmond, Phys. Rev. Lett. **80**, 5679 (1998).

[18] E. K. Wheeler, P. Fischer, and G. G. Fuller, J. Non-Newtonian Fluid Mech. **75**, 208 (1998).

[19] N. A. Spenley, M. E. Cates, and T. C. B. McLeish, Phys. Rev. Lett. **71**, 939 (1993).

[20] J. F. Berret, D.C Roux and G. Porte, J. Physique II **4**, 1261 (1994).

[21] P. D. Olmsted and C.-Y. D. Lu, Phys. Rev. E **56**, R55 (1997).

[22] R. G. Larson, Rheol. Acta **31**, 497 (1992).

[23] L. Becu, S. Manneville, and A. Colin, cond-mat/0402249.

[24] R. Bandyopadhyay, and A. K. Sood, Europhys. Lett. **56**, 447 (2001).

[25] J.-B. Salmon, A. Colin, and D. Roux, Phys. Rev. E **66**, 031505 (2002)

[26] J.-B. Salmon, S. Manneville, and A. Colin, cond-mat/0307609.

[27] A. S. Wunenburger, A. Colin, J. Leng, A. Arneodo, and D. Roux, Phys. Rev. Lett. **86**, 1374 (2001).

[28] A. Groisman and V. Steinberg, Nature **405**, 53 (2000).

[29] P. E. Cladis and W. van Saarloos in *Solitons in Liquid Crystals* (ed. L. Lam and J. Prost), Springer, New York (1992), pp. 136-137, find "director turbulence" in nematics in cylindrical Couette flow.

[30] P. Manneville, "The transition to turbulence in nematic

liquid crystals: Part 1, general review. Part 2, on the transition via tumbling, " Mol. Cryst. Liq. Cryst. **70** 223 (1981), (8th International Conference on Liquid Crystals, Kyoto, 1980).

[31] J. Dasan, T.R. Ramamohan, A. Singh and P.R. Nott, Phys. Rev. E **66**, 021409 (2002).

[32] S. Katz, and R. Shinnar, Chemical Engineering Science **25**, 1891 (1970).

[33] M. Grosso, R. Keunings, S. Crescitelli, and P. L. Maffettone, Phys. Rev. Lett. **86**, 3184 (2001).

[34] G. Rienäcker, M. Kröger, and S. Hess, Phys. Rev. E **66**, 040702(R) (2002).

[35] G. Rienäcker, M. Kröger, and S. Hess, Physica A **315**, 537 (2002).

[36] S. Hess and I. Pardowitz, Z. Naturforsch. **36a**, 554 (1981) discuss the hydrodynamics of a spatially inhomogeneous alignment tensor.

[37] A. Aradian and M. E. Cates, [cond-mat/0310660].

[38] A. Aradian and M. E. Cates, [cond-mat/0410509].

[39] P.T. Callaghan, M.E. Cates, C.J. Rofe, J.B.A.F. Smeulders, J. Phys. II France **6**, 375 (1996).

[40] M. D. Johnson, and D. Segalman, J. Non-Newt. Fluid Mech. **2**, 255 (1977).

[41] D. S. Malkus, J. A. Noehl, and B. J. Plohr, J. Comp. Phys. **87**, 464 (1990).

[42] F. M. Leslie, Quart. J. Mech. appl. Math. **19**, 357 (1966); Arch. ration. Mech. Analysis **28**, 265 (1968).

[43] J. L. Ericksen, Arch. ration. Mech. Analysis **4**, 231 (1960); Phys. Fluids **9**, 1205 (1966).

[44] D. Forster, T. C. Lubensky, P. C. Martin, J. Swift and P. S. Pershan, Phys. Rev. Lett. **26**, 1016 (1971).

[45] Orsay Group on Liquid Crystals. Mol. Cryst. Liq. Cryst. **13**, 187 (1971).

[46] P.C. Martin, O. Parodi and P.S. Pershan, Phys. Rev. A **6**, 2401 (1972); D. Forster, *Hydrodynamic Fluctuations, Broken Symmetry, and Correlation Functions*, Benjamin, Reading (1975).

[47] S. Hess, Z. Naturforsch. **30a**, 728 (1975);

[48] H. Stark and T.C. Lubensky, Phys. Rev. E **67** 061709 (2003).

[49] P. G. de-Gennes, *Simple views on condensed matter*, (World Scientific, Singapore, 1992).

[50] P.G. de Gennes, J. Prost, *The Physics of Liquid Crystals*, (Clarendon Press, Oxford, 1995).

[51] C. Pereira Borgmeyer, and S. Hess, J. Non Equil. Thermodyn. **20**, 359 (1995).

[52] G. Rienäcker, and S. Hess, Physica A **267**, 294 (1999).

[53] D. Forster, Phys. Rev. Lett. **32**, 1161 (1974).

[54] M. Doi, J. Polym. Sci. Polym. Phys. Ed. **19**, 229 (1981).

[55] P. D. Olmsted and P. M. Goldbart, Phys. Rev. A **41**, 4578 (1990).

[56] D. Chakraborti, *work in progress*.

[57] The disordered and ordered domains form geometrical patterns as seen in class 3 and 4 patterns in cellular automata.

[58] H. Chaté and P. Manneville, Physica D **32** 409 (1988).

[59] K. Kaneko, Prog. Theor. Phys. **74** 1033 (1985).

[60] M. van Hecke, Phys. Rev. Lett **80**, 1896 (1998).

[61] J. Rolf, T. Bohr, and M. H. Jensen, Phys. Rev. E **57**, R2503 (1998).

[62] T. M. Janaki, S. Sinha, and N. Gupte, Phys. Rev. E **67**, 056218 (2003).

[63] Y. Pomeau, Physica D **23**, 3 (1986).

[64] P. Rupp, Reinhard Richter, and Ingo Rehberg, cond-mat/0211137.

[65] H. Chaté and P. Manneville, Phys. Rev. Lett. **58**, 112 (1987).

[66] F. Daviaud, M. Bonetti, and M. Dubois, Phys. Rev. A., **42**, 3388 (1990).

[67] Ning-Ning Pang and N. Y. Liang, Phys. Rev. E, **56**, 1461 (1997).

[68] A. Pande, Ph D Thesis, Indian Institute of Science (2000) explores spatiotemporal chaos in a wide variety of systems.

[69] R. Hegger, H. Kantz, and T. Schreiber, CHAOS **9**, 413 (1999); *http://lists.mpipks-dresden.mpg.de/~tisean/*.

[70] M.B. Kennel, R. Brown, and H. D. I. Abarbanel, Phys. Rev. A **45**, 3403 (1992).

[71] J.-P. Eckmann and D. Ruelle, Rev. Mod. Phys. **57**(3), 617 (1985).

[72] R. Carretero-Gonzalez *et al.*, Chaos **9**, 466 (1999).

[73] S. Orstavik, R. Carretero-Gonzalez and J. Stark, Physica D **147**, 204 (2000).

[74] R. Carretero-Gonzalez and M. J. Bunner, preprint, *http://www-rohan.sdsu.edu/~rcarrete/publications/index.html*.

[75] D. Ruelle, Commun. Math. Phys., **87**, 287 (1982).

[76] Such a rescaling approach typically consists of studying the evolution of a relatively small N_s dimensional subsystem (which has the same equations of motion as the original, large, N dimensional system), and approximating the LS of the latter by rescaling the LS of the former by the ratio of the volumes N/N_s.

[77] M. Sano, and Y. Sawada, Phys. Rev. Lett. **55**, 1082 (1985).

[78] J. Mewis, M. Mortier, J. Vermant and P. Moldenaers, Macromol. **30**, 1323 (1997).

[79] J. Berghausen, J. Fuchs, and W. Richtering, Macromolecules **30**, 7574 (1997).